[This is a non-peer reviewed preprint submitted to EarthArXiv under review in the "International Journal of Applied Earth Observation and Geoinformation"]

Realistic and simplified models of plant and leaf area indices for a seasonally dry tropical forest

Rodrigo de Queiroga Miranda[1*], Rodolfo Luiz Bezerra Nóbrega[2,3], Magna Soelma Beserra de Moura[2,4], Raghavan Srinivasan[5], Josiclêda Domiciano Galvíncio[1]

[1]*Laboratório de Sensoriamento Remoto e Geoprocessamento, Universidade Federal de Pernambuco, Recife, Pernambuco, Brazil, 50670901, rodrigo.qmiranda@ufpe.br*

[2]*Department of Geography and Environmental Science, University of Reading, RG6 6AH Reading, UK*

[3]*Department of Life Sciences, Imperial College London, SL5 7PY Ascot, UK, r.nobrega@imperial.ac.uk*

[4]*Embrapa Tropical Semiarid, Petrolina, Pernambuco, Brazil, 56302970*

[5]*Spatial Sciences Laboratory, Texas A&M University, College Station, TX 77845, USA*

Abstract

The Leaf Area Index (LAI) has not been minimally calibrated for the seasonally tropical dry forest Caatinga in Brazil. LAI models that are currently used show satisfactory covariance when compared to *in situ* data, but they sometimes lack accuracy in the whole spectra of possible values and do not consider the impact that the stems and branches have over LAI estimates, which is of great influence in the Caatinga. In this study, we develop and assess PAI (Plant Area Index) and LAI models by using ground-based measurements and Landsat data. The objective of this study was to create and test new empirical models using a multi-year and multi-source of reflectance set of data. The study was based on measurements of photosynthetic photon flux density (PPFD) from above and below the canopy during the periods of 2011–2012 and 2016–2018. Through an iterative processing, we obtained more than a million candidate models for estimating PAI and LAI. To clean up the small discrepancies in the extremes of each interpolated series, we smoothed out the dataset by fitting a logarithmic equation with the PAI data and the inverse contribution of WAI (Wood Area Index) to PAI, that is the portion of PAI that is actually LAI (LAI_C). LAI_C can be calculated as follows: $\mathrm{LAI}_C = 1 - (\mathrm{WAI}/\mathrm{PAI})$). All of the WAI values were subtracted by the PAI to develop our *in situ* LAI dataset that was used for further analysis. Our *in situ* dataset was also used as a reference to compare our models with three other previously calibrated models for the Caatinga, as well as the MODIS-derived LAI products (MCD15A3H/A2H). Our main findings were as follows: (*i*) Six of those models use NDVI (Normalized Difference

Vegetation Index), SAVI (Soil-Adjusted Vegetation Index) and EVI (Enhanced Vegetation Index) as input, and performed well, with r^2 ranging from 0.77 to 0.79 (PAI) and 0.78 to 0.81 (LAI), and RMSE with a minimum of 0.42 m^2 m^{-2} (PAI) and 0.41 m^2 m^{-2} (LAI). The SAVI models showed values 20% and 32% (PAI), and 21% and 15% (LAI), smaller than those found for the models that use EVI and NDVI respectively. (*ii*) The other five models use only two bands, and in contrast to the first six models, these new models may abstract other physical processes and components, such as leaves etiolation and increasing protochlorophyll. The developed models used the NIR band, and they varied only in relation to the inclusion of the red, green and blue bands. (*iii*) All previously published models and MODIS-LAI underperformed against our calibrated models. Our study was able to provide several PAI and LAI models that realistic represent the phenology of the Caatinga.

Keywords: Caatinga, Landsat, phenology, semi-arid, Woody Area Index.

1. Introduction

The Leaf Area Index (LAI) is a widely adopted parameter in environmental sciences. It represents the one-sided area of leaves that covers a specific surface area (Fotis et al., 2018; Knote et al., 2009; Mu et al., 2007; Rodriguez et al., 2009) and is one of the main parameters of both global and regional biosphere models (Arnold et al., 1998; Bieger et al., 2017). LAI is used to scale up from vegetation photosynthesis and transpiration, energy balance of terrestrial surfaces, and many climatological and hydrological attributes such as atmospheric aerosols, water infiltration, and biogeochemical processes (Bonan, 1995).

There are two main approaches used to estimate LAI: (*i*) direct methods, in which the total leaf canopy is obtained by the summation of direct measurement of all individual leaf areas – this is usually a destructive method because it requires the removal of all leaves and, therefore, is not viable at large scales; and (*ii*) indirect methods, which require active or passive sensors to measure parameters that are highly correlated with LAI, such as light extinction coefficient. Active sensors do not depend on solar radiation; they emit their own electromagnetic signals and capture those reflected. Passive sensors depend on solar radiation and are based on estimating the extent to which a given amount of leaf area will reduce radiation transmitted through a stratified arrangement of leaf elements within a canopy. This estimation can be determined using a radiative transfer model such as the PROSPECT and SAIL models (Jacquemoud et al., 2009; Jacquemoud and Baret, 1990; Knyazikhin et al., 1998; Verhoef, 1985, 1984) or abstracted by coefficients of an empirical model (Bastiaanssen, 1998; Galvíncio et al., 2013; Machado, 2014).

Radiative transfer models are highly accurate, but require specific inputs, such as pigment concentration, cell diameter and water content (Jacquemoud et al., 2009; Jacquemoud and Baret, 1990). These parameters can only be obtained with extensive fieldwork, while empirical models are purely statistical fast retrieval algorithms. To estimate LAI, the empirical models are mainly composed of regressions that relate simple spectral responses and greenness indices (Galvíncio et al., 2013; Machado, 2014), such as the Soil Adjusted Vegetation Index ($SAVI$) and Normalized Difference Vegetation Index ($NDVI$) (Bastiaanssen, 1998; Galvíncio et al., 2013), to the LAI. For LAI estimations at a regional scale, empirical models are generally reliable (Knote et al., 2009). However, in Brazil, more specifically in the seasonally dry tropical forest in the semiarid region, the Caatinga, models that are currently used have not been calibrated using emporal field measurements.

The Caatinga is the largest continuous seasonally dry tropical forest (SDTF) in the Americas, with an open and mostly semi-arid landscape, as seen in many interplateau depressions (Ab'Saber, 1974; Silva et al., 2017). The Caatinga covers an area of approximately 900,000 km^2 (Silva et al., 2017). Its climate is characterized by high temperatures and low rainfall rates with high intra- and inter-annual variability both in space and time. The rainfall is normally concentrated over 2–4 months of the year, with the possibility of over 25% of the annual precipitation occurring in a single rainfall event (Miranda et al., 2018). The Caatinga holds over 3,150 species of 930 genera and 152 families of flowering plants (Silva et al., 2017). These plants have unique adaptations to endure conditions of spatiotemporally irregular water availability and extended droughts: approximately 85% of the Caatinga species lose all their leaves during an average dry season (Silva et al., 2017). Thus, methods that attempt to measure the LAI by directly relating it to the intercepted radiation do not be reflect only the area of the leaves, but also the surface of the woody area mainly comprised of stems and branches (Cunha et al., 2019). The influence that stems and branches have over the LAI estimates can be addressed by computing the LAI as the difference between Plant Area Index (PAI) and the Woody Area Index (WAI).

Currently, model estimates of LAI in the Caatinga show satisfactory covariance when compared to *in situ* data (Galvíncio et al., 2013; Machado, 2014), but they lack accuracy in the entire spectra of possible values because they are often calibrated with spatial data from a single day, neglecting temporal variations due to phenology. Vegetation indices often have a determined range of values. In addition, models applied to the Caatinga have not considered the influence of the WAI, which is highly significant in the Caatinga as over 85% of plant's above-ground biomass is composed of stems and branches (Silva and Sampaio, 2008). The oversight of this uniqueness of the Caatinga vegetation induces to methodological flaws because only a minimum phenological change are reproduced to the Caatinga.

In this study, we aimed to create and test new empirical models using a multi-year and multi-source set of reflectance data. We rely on the premise that by providing multiple reflectance data combinations as input, and accounting for the WAI component of the PAI, we will be able to provide models that are more accurate and better adjusted to the Caatinga. Our objectives were to evaluate the efficiency of new LAI models derived from Landsat reflectance using fitted models and field measurements from a typical Caatinga formation area in Brazil, and to test new empirical models using previously published models currently used for the Caatinga.

Study area

Data were collected in an area of shrub hyperxerophytic Caatinga forest area (Fig. 1) (Kiill, 2017), located at the Embrapa Tropical Semiarid Research Station in the state of Pernambuco, Brazil (9°2'33"S, 40°19'16"W; at 350 m a.s.l.). The vegetation in this area consists of shrubs, trees, herbaceous plants, and Cactaceae. The canopy average height is 4.5 m. The dominant species (approximately 90% of the total relative dominance) are *Commiphora leptophloeos*, *Schinopsis brasiliensis*, *Mimosa tenuiflora*, *Cenostigma microphyllum*, *Sapium glandulosum*, *Cnidosculus quercifolius*, *Handroanthus spongiosus*, *Manihot pseudoglaziovii*, *Croton conduplicatus*, and *Jatropha mollissima* (Kiill, 2017). Although the Cactaceae (*Pilosocereus gounellei* and *Pilosocereus pachycladus)* have a fairly constant phenological status throughout the year, these plants have a relative dominance of less than 5% and an insignificant production of leaves; therefore they were not considered in our LAI estimates. The climate is dry semi-arid (Alvares et al., 2013), with the rainy season between January and April and an average annual temperature of 26°C. Although the average historical annual rainfall is approximately 500 mm, the average rainfall was less than 300 mm during our study period, which is the greatest drought in this region’s recorded history. These conditions were particularly interesting for our study, allowing a precise assessment of the WAI influence on the total PAI.

[This is a non-peer reviewed preprint submitted to EarthArXiv under review in the “International Journal of Applied Earth Observation and Geoinformation”]

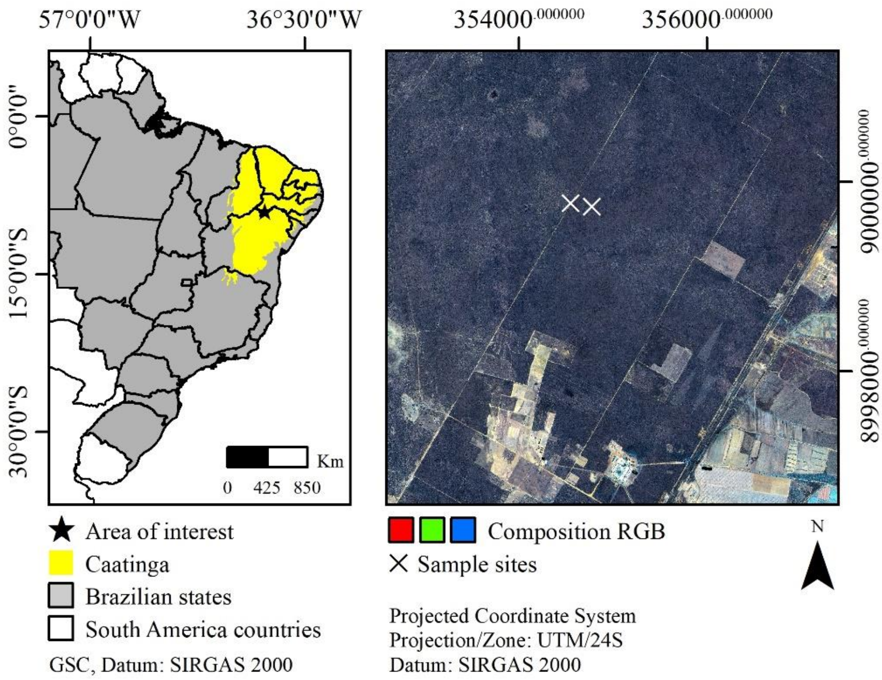

Figure 1 - Location of the dry forest experimental area at the Embrapa Semiarid Research Station in the state of Pernambuco (Brazil).

2. Methodology

Field measurements

LAI was derived from field measurements of photosynthetic photon flux density (PPFD) taken from above and below the canopy using two different non-destructive methods. The obtained measurements composed the final dataset, covering a period of 5 years: 2011–2012 and 2016–2018. The first method measured PPFD using three quantum sensors (one LI-190SA sensor to measure the above-canopy PPFD, and two LI-191 sensors for the below-canopy data) installed in a 16-m meteorological tower in the study area. All sensors were connected to a data acquisition system (CR1000, Campbell Scientific Inc.), which was programmed to compute averages of 30-s measurements taken at 30-min intervals from January 2011 to December 2012. In order to maximize the quality of our measurements, we filtered all data, considering only the average of the measurements between 10 am and 2 pm each day (GMT -3), when the zenith angle is close to zero. The second measurement approach was applied on a weekly basis (68.97% of the entire dataset) from January 2016 to November 2018, with exceptions: 19.54% (≥ 8 days of interval between measurements – DBM), 8.05% (≥ 14 DBM) and 3.45% (≥ 21 DBM). The dataset consisted of LAI estimates based on the transmission of light through the canopy at various angles by using an AccuPAR ceptometer (AccuPAR® LP-80, Decagon Devices). The AccuPAR has a linear ceptometer with 80 sensors, capable of measuring PPFD at the photosynthetically active radiation (PAR) range (400–700 nm wavelength), from 0 to 2500 μmol m^{-2}. The above-canopy PPFD and solar zenith angle measurements were obtained in a nearby (about 10 m away) clear area, and the below-canopy PPFD was acquired by holding the AccuPAR beneath the canopy at approximately 0.4 m above ground. The dataset from this approach was linearly interpolated to produce the daily data required to match the satellite overpass times. We used the data collected to predict scattered and transmitted PPFD, as well as to predict light extinction, as proposed by Norman (1979).

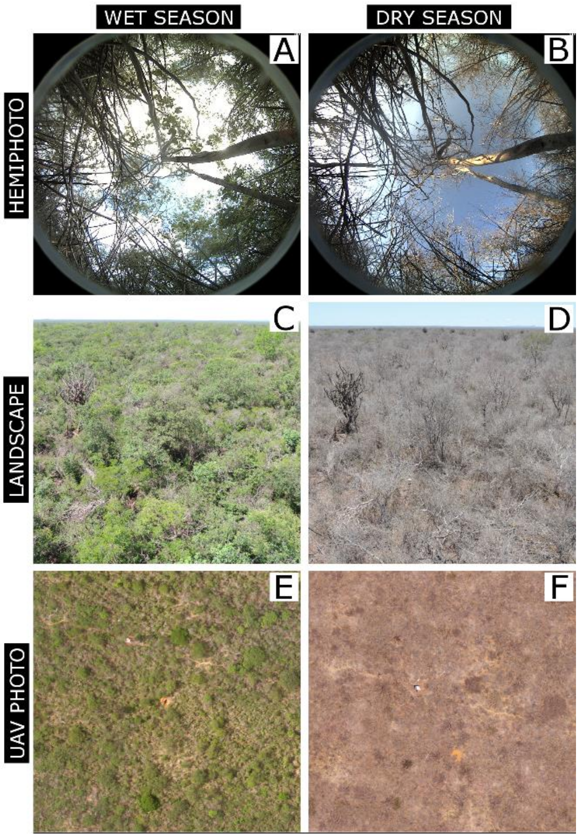

Figure 2 - Contrast in the Caatinga between its wet (A, C and E) and dry (B, D and F) conditions. A–B are hemispheric photos taken from below the vegetation in 12/18/2018 and 9/27/2018 respectively; C–D are landscape photos taken horizontally in 2/5/2016 and 10/20/2017 at a height of 14 m; E–F are orthophotos taken by drone (unmanned aerial vehicle) at 80 m height in 02/16/2018 and 10/20/2017, respectively.

Plant Area Index (PAI) partitioning

In our study, we defined PAI as the sum of WAI and LAI (Magalhães et al., 2018), and the WAI as the contribution of woody material such as stems, branches and trunks to the light interception of PAI. In order to carry out this partition of our data, we first took the minimum LAI (LAI_{MIN}) value of each year as the WAI, which was verified by visual evaluation of hemispheric photos from a phenological monitoring database (Fig. 2); then we fixed this value from the day of the LAI_{MIN} to the first subsequent day with rainfall over 2.5 mm. Based on field observations, we assumed that low-precipitation ($\leq$ 2.5 mm d^{-1}) events do not cause any significant phenological change in the ecosystem. The WAI was assumed to gradually change between sequential dry seasons; we gap-filled the WAI dataset with a linear interpolation between the fixed-value periods of each year. To avoid small discrepancies in the extremes of each interpolated series, we smoothed the dataset by fitting a logarithmic equation (Eq. 1) with the PAI data and the inverse contribution of WAI to PAI, which is the percentage of PAI that is actually LAI (here called LAI_C). LAI_C can be calculated as follows: $\mathrm{LAI}_C = 1 - (\mathrm{WAI}/\mathrm{PAI})$. The WAI values were subtracted from the PAI to develop our *in situ* LAI dataset, which is used for further analysis.

$$\mathrm{WAI} = \{1 - [\ln(\mathrm{PAI}) \times 0.5]\} \times \mathrm{PAI} \tag{1}$$

Landsat data processing

We selected the Landsat Surface Reflectance Level-2 products for the entire study period (total of 110 candidate images). These products are designed to provide atmospherically and geometrically corrected reflectance data with a 30-m resolution every 16 days. These data are generated using the auxiliary climate data from MODIS (e.g., water vapor, ozone, geopotential height, and aerosol optical thickness) and two different algorithms: 1) the Second Simulation of a Satellite Signal in the Solar Spectrum (6S) algorithm to the data derived from Landsat 5 Thematic Mapper (TM) and Landsat 7 Enhanced Thematic Mapper Plus (ETM+) images; and 2) a unique radiative transfer model to the Landsat 8 Operational Land Imager (OLI) data. The data were extracted from two sample sites (Fig. 1), and all clear pixels were filtered using the respective Quality Band (QA band) of each product (L5–7 = 66, and L8 = 322), resulting in a 70-record dataset. The dataset was then submitted to an iterative model-fitting approach to create new PAI and LAI models. The

Landsat L2-level products include reflectance values derived from three sensors (TM/Landsat 5, ETM+/Landsat 7, and OLI/Landsat 8) with 30-m spatial resolution. The different bands were matched to create an equivalent dataset of reflectance across all sensors (Table 1). These products are freely available through the LSDS Science Research and Development (LSRD) database of the U.S. Geological Survey (https://espa.cr.usgs.gov/).

OLI/Landsat 8 (nm)	ETM+/Landsat 7 and TM/Landsat 5 (nm)	Equivalent bands for this study (nm)
-	$\rho_1^{ETM+/TM}$= 450–520	$\rho_1 = [\rho_2^{OLI}, \rho_1^{ETM+/TM}]$
ρ_2^{OLI}= 452–512	$\rho_2^{ETM+/TM}$= 520–600	$\rho_2 = [\rho_3^{OLI}, \rho_2^{ETM+/TM}]$
ρ_3^{OLI}= 533–590	$\rho_3^{ETM+/TM}$= 630–690	$\rho_3 = [\rho_4^{OLI}, \rho_3^{ETM+/TM}]$
ρ_4^{OLI}= 636–673	$\rho_4^{ETM+/TM}$= 770–900	$\rho_4 = [\rho_5^{OLI}, \rho_4^{ETM+/TM}]$
ρ_5^{OLI}= 851–879	$\rho_5^{ETM+/TM}$= 1,550–1,750	$\rho_5 = [\rho_6^{OLI}, \rho_5^{ETM+/TM}]$
ρ_6^{OLI}= 1,566–1,651	-	-
ρ_7^{OLI}= 2,107–2,294	$\rho_7^{ETM+/TM}$= 2,090–2,350	$\rho_7 = [\rho_7^{OLI}, \rho_7^{ETM+/TM}]$

Table 1 - Equivalence table of the bands of the sensors TM/Landsat 5, ETM+/Landsat 7 and OLI/Landsat 8.

Model calibrations

We developed PAI and LAI models based on the combinations of bands (ρ_1 to ρ_7); vegetation indices ($NDVI$, $SAVI$ and EVI; Eqs. 2 to 4); transformation functions, i.e., x, $1/x$, $\ln(x)$, $\log_{10}(x)$, $\sqrt{x}$, x^2, e^x; and basic mathematical operations. These models were obtained by using an exhaustive training iteration process (> 10^6 iterations) that selected the best results based on the highest coefficient of determination (r^2) with the lowest Root Mean Square Error (RMSE). We used the Percent Bias (PBIAS) and concordance correlation coefficient (ρ_c) as auxiliary performance indices. We obtained $NDVI$, $SAVI$ and Enhanced Vegetation Index (EVI) using Eqs. 2 to 4, where $C1$ (6) and $C2$ (7.5) are the coefficients of the aerosol resistance, G (2.5) is a gain factor, and L is the soil effect constant, according to Rouse et al. (1974) and Huete (1988). Our L for the EVI was set to 1 according to Jiang et al. (2008), while for the L in the $SAVI$ we performed a sensitivity analysis, varying the factor L

from -1 to 1 with intervals of 0.01. The best L-value occurred when simulated data achieved the highest r^2 with the lowest RMSE, and these values were 0.07 (for the PAI) and 0.37 (for the LAI). The number of models evaluated can be calculated using Eq. 5, where nc is the number of parameters entered into the model. All independent data were previously tested with the Variance Inflation Factor ($VIF = 1/(1 - \mathrm{r}^2)$) to avoid any significant multicollinearity. We considered data to be independent when $VIF < 10$. All processing was performed using an interpreter Python 2.7.15 with only basic modules installed (freely available at (https://github.com/razeayres/correlator).

$$NDVI = \left(\frac{\rho_4 - \rho_3}{\rho_4 + \rho_3}\right) \tag{2}$$

$$SAVI = \frac{(1 + L) \times (\rho_4 - \rho_3)}{L + \rho_4 + \rho_3} \tag{3}$$

$$EVI = G \times \frac{\rho_4 - \rho_3}{\rho_4 + C1 \times \rho_3 - C2 \times \rho_1 + L} \tag{4}$$

$$\begin{gathered} f(nc) = C^{nc}_{\begin{bmatrix} \rho_1 & \rho_4 & NDVI \\ \rho_2 & \rho_5 & SAVI \\ \rho_3 & \rho_7 & EVI \end{bmatrix} + (nc-1)} \times C^{nc}_{\begin{bmatrix} x & {}^{1}/_{x} & \ln(x) \\ \log_{10}(x) & \sqrt{x} & x^2 \\ e^x & & \end{bmatrix} + (nc-1)} \\ \times \begin{cases} 1, & nc = 1 \\ C^{(nc-1)}_{\begin{bmatrix} + & - \\ \times & \div \end{bmatrix} + (nc-2)}, & nc \geq 2 \end{cases} \end{gathered} \tag{5}$$

Models verification

To verify the accuracy of all models in this study, we first assessed the applicability of parametric statistics to all data with the Shapiro–Wilk (for normality) and Brown–Forsythe (for homoscedasticity) tests (Zar, 1996), and then we conducted a comparison between the remotely sensed data and the estimates from the field observations using the Monte Carlo cross-validation technique (Xu and Liang, 2001), considering 91 different sampling sizes varying from 5 to 95% of the total data at 1% intervals. Each sample was evaluated by its r^2 and computed as the mean of 50 random repetitions. The methods of cross-validation are widely adopted, and they were used to check whether models tend to over-adjust to the *in situ* dataset distribution (Hawkins, 2004). This over-adjustment would mean that excellent results would be obtained only in calibration (Shao, 1993), while during verification, the accuracy of the model would drastically drop. This approach allows for a good calibration (Shao, 1993). In addition, we compared our field observations and verified models to the LAI models proposed by Bastiaanssen (1998) (Eq. 6), Galvíncio et al. (2013) (Eq. 7), and Machado (2014) (Eq. 8) and derived from MODIS data (MCD15A3H/A2H). These models may produce excellent independent data required for model prediction testing.

$$LAI = -\frac{\ln\left[{(0.69 - SAVI)}/{0.59}\right]}{0.91} \tag{6}$$

$$LAI = e^{1.426 + \frac{-0.542}{NDVI}} \tag{7}$$

$$LAI = 0.102 \times e^{5.341 \times NDVI} \tag{8}$$

For Eqs. 6 to 8, we used the same Landsat dataset produced for the models calibrations; for the MODIS MCD15A2H/A3H products, we used all images for the entire study period (total of 830 images). These products are designed to provide data with a spatial resolution of 500 m every 4 days (MCD15A3H) or every 8 days (MCD15A2H). They are based on a complex algorithm that uses both the daily surface reflectance values of the MODIS sensor on one or both of the Terra and Aqua satellites and the data from a radiative transfer model, which are stored in a two-dimensional lookup table (Yang et al., 2006). These reflectance data are already corrected for atmospheric interferences such as atmospheric gases and aerosols, and they are freely available through the Earth Explorer online tool of the U.S. Geological Survey (https://earthexplorer.usgs.gov/). For all products, scale corrections were performed using the Geospatial Data Abstraction Library and clear land dry forest pixels were filtered using the Quality Band (QA band, value 0).

3. Results and discussion

Six of our selected models use $NDVI$, $SAVI$ and EVI as input (Eqs. 14 to 16 and 22 to 24 in Table 2). These models exhibited r^2 values ranging from 0.77 to 0.79 for PAI and 0.78 to 0.81 for LAI, and RMSE with a minimum of 0.41 m^2 m^{-2} for PAI, and 0.40 m^2 m^{-2} for LAI. The $SAVI$ models (Eqs. 14 and 22) showed RMSE values smaller than the ones found for the models that use EVI and $NDVI$. We ascribe the better accuracy with the $SAVI$ models for both r^2 and RMSE over the other vegetation indices to the fact that $SAVI$ is the only one that takes into consideration the effects of soil background, allowing for better estimates for soil exposure under the vegetation of the Caatinga. In addition, $SAVI$ better reflects the surface roughness, which affects momentum, heat, and water vapor fluxes (Bastiaanssen, 1998) and varies according to the phenological stages in the Caatinga (Teixeira et al., 2008). These models are interesting because they allow easy retrieval of the PAI or LAI from remote sensing data. For example, many $NDVI$ products, using a large variety of sensor data, are freely available, and they can be used to acquire physical information for extended forest areas.

Our models presented a better performance when fitted linearly rather than logarithmically. This is the opposite of what was shown by some $NDVI$–LAI relationship models (Liu et al., 2012; Tavakoli et al., 2014). Liu et al. (2012) conducted an experiment in the Ningxia Hui Autonomous District, one of the most drought-prone areas in Northwest China. They focused on the quantification of saturation of $NDVI$ saturates at high LAI values. Tavakoli et al. (2014), in 16 plots of winter wheat (*Triticum aestivum* L., cv. Cubus) in an experimental station located in Marquardt in Germany, found the best $NDVI$–LAI relation when fitting data logarithmically. In fact, this saturation of LAI in function of $NDVI$ is commonly expressed by a logarithmic relationship. In our study, the Caatinga vegetation did not exhibit saturation related to the vegetation indices values, resulting in a linear covariance.

Absolute simulated LAI values varied from 0 to 4.55 m^2 m^{-2} (0.61 to 5.23 m^2 m^{-2} for PAI values).From those, Bastiaanssen (1998) exhibited values from 0.1 to 4.45 m^2 m^{-2}, Galvíncio et al. (2013) from 0.63 to 1.98 m^2 m^{-2}, and Machado (2014) from 0.25 to 3.7 m^2 m^{-2}. Bastiaanssen (1998) derived LAI using different equations for only six types of land use (cotton, corn, soy, wheat, fruit trees, and vegetables), none of which were similar to the dry forest in our study area. The experiment of Galvíncio et al. (2013) was based on a comparison of data obtained using an AccuPAR analyzer with indices created from spectroradiometry. The resulting models were later verified using IKONOS images with 1-m spatial resolution (Galvíncio et al., 2013) and TM/Landsat 5 data with 30-m spatial resolution (Machado, 2014). The model proposed by Machado (2014) was developed in a Caatinga area of the National Park of Catimbau using a Landsat 5 TM image combined with 54 field-derived LAI measurements acquired using simultaneous averages of diffuse light interception at five different zenith angles using sensors with fisheye lens.

	Model		r^2 [1]	RMSE [2]	ρ_c	PBIAS [2]
PAI	Eq. 9	$y = 10.1 \times (\rho_4 - \sqrt{\rho_3}) + 3.1$	0.79	0.41	0.88	0.33
	Eq. 10	$y = -13.2 \times (\sqrt{\rho_2} - \rho_4) + 3.1$	0.77	0.44	0.87	1.84
	Eq. 11	$y = -13.5 \times \left({\log_{10}(\rho_4)}/{\ln(\rho_3)}\right) + 6.1$	0.77	0.43	0.87	-1.84
	Eq. 12	$y = -20.3 \times (\rho_3 - {\rho_4}^2) + 3$	0.77	0.43	0.87	-0.83
	Eq. 13	$y = -3.2 \times (\ln(\rho_3) \times \sqrt{\rho_4}) - 1.4$	0.79	0.41	0.88	-0.22
	Eq. 14 [3]	$y = 3.5 \times (e^{SAVI}) - 2.7$	0.79	0.41	0.88	1.10
	Eq. 15	$y = 4.8 \times (e^{EVI}) - 3.7$	0.77	0.45	0.86	3.72

	Eq. 16	$y = 5 \times (NDVI^2) + 1.3$	0.79	0.43	0.89	1.04
LAI	Eq. 17	$y = \left({\rho_4}^2/\rho_1\right) - 0.1$	0.79	0.41	0.88	-0.01
	Eq. 18	$y = -9.7 \times \left(\log_{10}(\rho_3) / \left(\frac{1}{\rho_4}\right)\right) - 1.2$	0.78	0.42	0.88	-4.84
	Eq. 19	$y = 11.2 \times \left(\sqrt{\rho_4} - e^{\rho_3}\right) + 8.3$	0.76	0.44	0.86	7.15
	Eq. 20	$y = 12.2 \times \left(\sqrt{\rho_4} - \sqrt{\rho_2}\right) - 1.2$	0.76	0.44	0.86	-0.73
	Eq. 21	$y = 19.6 \times ({\rho_4}^2 - e^{\rho_3}) + 21.4$	0.78	0.42	0.87	-3.01
	Eq. 22 [3]	$y = 11 \times (SAVI^2) + 0.2$	0.81	0.40	0.89	0.04
	Eq. 23	$y = 6.5 \times (EVI) - 0.4$	0.78	0.42	0.88	-5.71
	Eq. 24	$y = 4.9 \times (NDVI^2) + 0.1$	0.80	0.41	0.89	4.39

[1] Significant at $p = 0.05$
[2] RMSE is in $m^2\ m^{-2}$, and PBIAS is showed as percentage.
[3] L-values in the $SAVI$ calculations were 0.07 (for the PAI) and 0.37 (for the LAI).

Table 2 - Calibration of PAI and LAI models created through an iterative process using Landsat reflectance data.

The best-performing new models that use different band combinations were Eqs. 9 to 13 and 17 to 21 (Table 2). These equations may represent other physical processes and components, such as leaf etiolation and increasing protochlorophyll, which is reported to influence the blue band of the visible spectrum (ρ_1 in Eq. 17) (Gates et al., 1965). Our models used the NIR band, and they varied only to the inclusion of the red, green and blue bands. The amount of energy reflected or absorbed in these bands varies according to the physicochemical and biophysical properties of the target. All bodies reflect or emit electromagnetic radiation at different wavelengths and in different ways, and the result is a reflectance curve or spectral signature. This set of unique interactions restricts the bands that distinguish certain characteristics of a target and allows various parameters quantification (e.g., pigment concentration and plant structure complexity). The NIR band has a strong interaction with plant biodiversity in a complex ecosystem as the Caatinga. Medeiros et al.

(2019) suggested the NIR band may be a good indicator of leaf radiation reflectance patterns among different species. Usually, vegetation reflects about half of the incident radiant flux in the NIR band (Zhao et al., 2007); therefore, this is a band very sensitive to biomass and LAI. Leaves predominantly absorb energy from the blue–red spectrum and reflect the energy in the green and NIR bands because of the interaction with chlorophyll, carotenoids and the mesophyll itself (Gates et al., 1965). Thus, the green and NIR bands can be considered to be bands of high reflectance, with NIR considerably less transparent than green because of the comparatively greater internal scattering of radiation in the leaves (Gates et al., 1965).

We consider Eqs. 9, 14 and 16 to be the optimal solutions for the estimation of PAI in the Caatinga, and Eqs. 17, 22 and 24 to estimate LAI (Table 2). Although studies have highlighted the dubious quality of data acquired by remote sensing in the blue band because of wavelength-dependent atmospheric interference (e.g., Carter et al., 2009; Motohka et al., 2009), Eq. 17 has performed very well with r^2 = 0.79 and RMSE = 0.41 m^2 m^{-2}, with values comparable to Eq. 22 (which does not use the blue band) with r^2 = 0.81 and RMSE = 0.40 m^2 m^{-2}. The greatest contribution of Eq. 17 is its natural proximity to a 1:1 relation to *in situ* measurements (ρ_c = 0.88, PBIAS = -0.01), which provides greater ability to simulate values near to zero. Although our models require observations in the NIR band, many images have NIR sensors and, if well calibrated, they allow for LAI to be estimated based on reflectance from spectral mixture or coarse resolution compositions. These images include those captured by phenological cameras, unmanned aerial vehicles, and high-resolution monitoring satellites (e.g., QuickBird and IKONOS).

The accuracy of our best models can be visualized when plotting their estimates alongside observed PAI and LAI data (Fig. 3). Our best performance models were able to satisfyingly emulate the variance of LAI in our study period. Eqs. 9, 14 and 22 are biased towards overestimation (PBIAS = 0.33, 1.10 and 0.04 respectively) and Eq. 17 presented a small underestimation bias (PBIAS = -0.01). In general, based on our findings, models developed with independent bands of a sensor produced low-magnitude values near optimal zero, indicating accurate model simulation, while the models created using vegetation indices exhibited moderate bias.

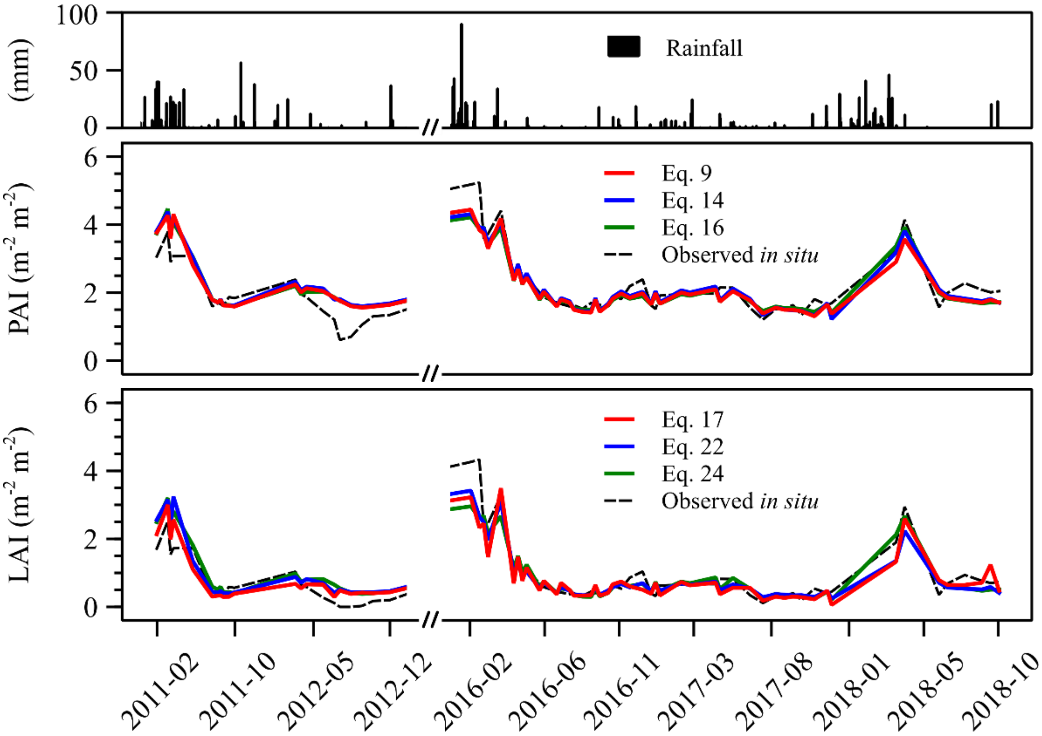

Figure 3 - Comparison of temporal variation of PAI (in the middle) and LAI (bottom) observed *in situ* to the best simulated models created through an iterative process using Landsat reflectance data.

In the cross-validation analyses, Eq. 9 produced maximum values (r_{max} = 0.81) and minimum values (r_{min} = 0.68) similar to Eq. 17 (r_{max} = 0.83, and r_{min} = 0.59). In comparison, the $NDVI$, $SAVI$ and EVI models yielded higher maximum and minimum values for both PAI (r_{max} = 0.83, 0.82 and 0.80, respectively; r_{min} = 0.73 for all models) and LAI (r_{max} = 0.84, 0.85 and 0.83; r_{min} = 0.71, 0.71 and 0.69, respectively). The other models presented r values ranging from 0.64 to 0.84 (for PAI), and 0.6 to 0.83 (for LAI). The 0.01

standard deviation of r was the same for all models, indicating that the models are reliable. When varying the amount of data taken for cross-validation from 5 to 95%, the r values tend to show minimal variations (Figs. 4 and 5). However, in our verification we did not observe any statistically significant pattern in correlation owing to the removal of data from the calibration of the models, which confirms that these models are highly robust to estimate LAI.

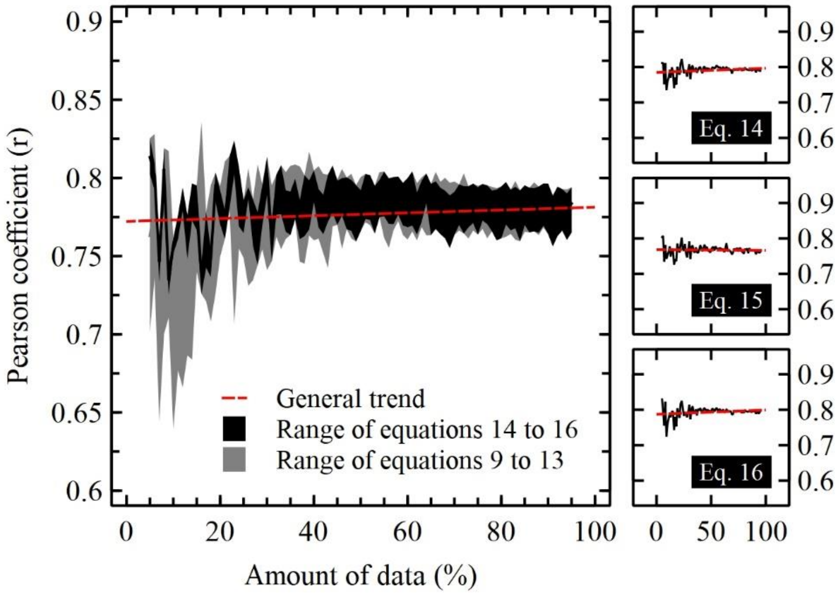

Figure 4 - Cross-validation of the PAI models created through an iterative process using Landsat reflectance data. Detailed validations of Eq. 14 to 16 are on the right side.

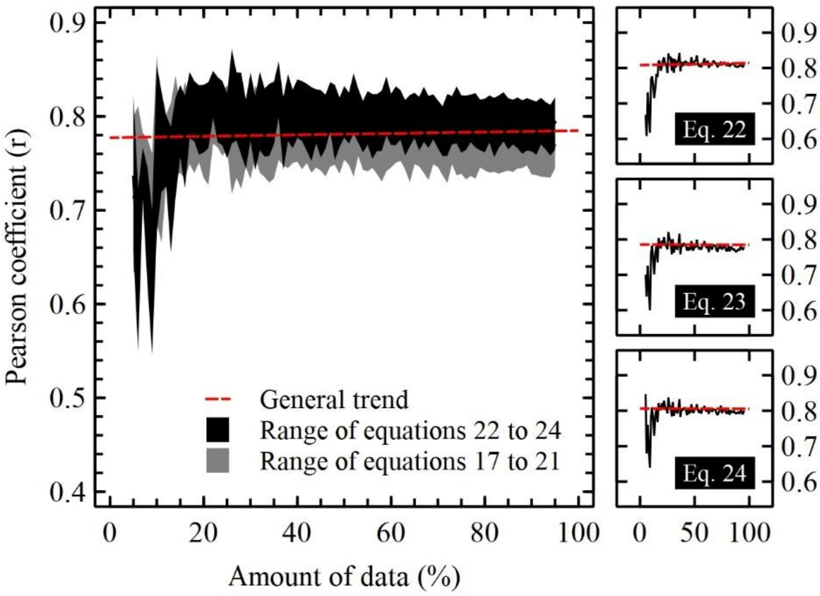

Figure 5 - Cross-validation of the LAI models created through an iterative process using Landsat reflectance data. Detailed cross-validations of Eqs. 22 to 24 are on the right side.

The approaches proposed by Bastiaanssen (1998) (Eq. 6), Galvíncio et al. (2013) (Eq. 7), and Machado (2014) (Eq. 8), as well as the MCD15A3H/A2H data underperformed compared to our models, when compared to our *in situ* PAI and LAI data (Table 3), even though correlations were significant ($p < 0.05$). The Eqs. 6 and 7 performed better in terms of accuracy, while Eq. 8 presented the highest covariance. Although the MODIS products are supposed to well reproduce the LAI seasonality, we observed that they do not respond well for the Caatinga during the dry season; the lowest values were around 0.5 $m^2\ m^{-2}$ when real LAI were practically zero. We tested the fitness of MODIS products against our *in situ* PAI and LAI datasets. The lower correlation with the MCD15A3H product in comparison to the MCD15A2H product indicates that the proportion of high-quality data for the dry forest area is lower for periods of composition of 4 days than for the 8-day version (Table 3). These periods of composition are created from the highest value observed *in situ*; thus, the greater the number of values available for the determination of LAI of each pixel, the higher the probability of it being an accurate value. This is because data obtained by satellites are influenced by a number of different atmospheric factors such as water vapor, cloud cover, and aerosols, so any given bit of satellite data may not yield accurate results (Yang et al., 2006). Regardless of their uncertainty, MODIS-LAI products have high temporal resolution and data availability and can still provide acceptable estimates for the Caatinga for some purposes, such as hydrological and soil–plant–atmosphere modelling, if carefully used during the wet season. However, studies that rely on LAI from MODIS products for regional vegetation assessment are likely to incorporate bias due to the unrealistically high LAI values during the dry season, which has direct consequences for the evapotranspiration or gross primary productivity estimates.

Reference	Parameter	r^2 [1]	RMSE [2]	ρ_c	PBIAS [2]
Bastiaanssen (1998)	PAI	0.73	1.54	0.35	-69.44
	LAI	0.75	0.51	0.84	-26.53
Galvíncio et al. (2013)	PAI	0.73	1.32	0.33	-57.44
	LAI	0.72	0.52	0.75	2.33
Machado (2014)	PAI	0.76	1.28	0.61	-40.48
	LAI	0.78	1.01	0.72	43.12
MCD15A3H	PAI	0.66	1.39	0.29	-60.08
	LAI	0.65	0.57	0.71	-4.00
MCD15A2H	PAI	0.77	1.26	0.38	-55.07
	LAI	0.78	0.46	0.82	8.04
Summary of selected models					
Eq. 9	PAI	0.79	0.41	0.88	0.33
Eq. 14 [3]	PAI	0.79	0.41	0.88	1.10
Eq. 16	PAI	0.79	0.41	0.89	1.04
Eq. 17	LAI	0.79	0.41	0.88	-0.01
Eq. 22 [3]	LAI	0.81	0.40	0.89	0.04
Eq. 24	LAI	0.80	0.41	0.89	4.39

[1] Significant at $p = 0.05$
[2] RMSE is in m^2 m^{-2}, and PBIAS is showed as percentage.
[3] *L*-values in the *SAVI* calculations were 0.07 (for the PAI) and 0.37 (for the LAI).

Table 3 - Comparison of the previously published models, and the MCD15A3H/A2H products with *in situ* data.

The LAI in this study, as seen in all models for the Caatinga, can be defined as effective LAI, which is the portion of LAI that effectively intercepts the light, not directly considering grouped foliage. This grouping of leaves can be quantified by a vegetation dispersion parameter Ω (clumping index) (Nilson, 1971), which often can be determined by a random distribution (Chen and Black, 1992). The "true" LAI is not easy to achieve, and requires intensive fieldwork and systematic sampling, using all possible allometric relationships (Frazer et al., 1997; Weiss et al., 2004), and since the approaches of estimating PAI and LAI used in our study are based on the light extinction, the WAI values as a result of the difference of PAI and LAI are likely to be underestimated when LAI is high (Nackaerts et al., 2000; Stenberg, 1996). This is attributed to the fact that when LAI values are very high, the leaves cover the woody area and reduce the role of light interception of the branches and steams (Chen et al., 1997), which in turn leaves the PAI and LAI values very similar (e.g., Feb 2012 in Fig. 3).

Our models are easy-to-use PAI and LAI predictors that can be applied to estimate these indices for the Caatinga. The models also can be used to simulate other Caatinga types (such as in transitional areas), but since they rely on calibration coefficients, minor adjustments might be required to approximate minimum and maximum LAI. Regional applicability can be considered as moderate-high, because the shrub phyto-physiognomy is probably the main and most abundant Caatinga type (Silva et al., 2017). However, at a regional scale, our models may be used as backup models in a physical approach that does not require calibration to achieve maximum generalization. Further improvements may include (*i*) pooling coefficients adjusted for other areas of Caatinga with different levels of degradation, which could be similar to what was made by Bastiaanssen (1998) when developing LAI models; (*ii*) the adjustment of these equations using field data from other types of Caatinga vegetation, where some plants, such as Cactaceae and Bromeliaceae, may have a more significant presence, and the soil exposure may be different; (*iii*) the removal of the influence of non-photosynthetic plant material, such as flowers, fruits and petioles, on LAI measurements; and (*iv*) approximation of LAI to more realistic values, developing and introducing a new *Ω* to more efficiently account for leaf dispersion directly in the models, instead of abstracting it in regression coefficients. This could solve systematic problems, such as misestimation of LAI at a given phenological stage.

4. Conclusions

Our study developed and assessed several PAI and LAI models to be realistically representative for the phenology of a typical Caatinga ecosystem. The joint usage of ground and satellite data presented an efficient way to assess both PAI and LAI models. The results included parameterizations that use the visible and infrared spectrum, which allowed the use of many currently available datasets to estimate LAI.

The models produced results with high accuracy (up to $r^2 = 0.81$ and RMSE = 0.41 m^2 m^{-2}). The significant improvement of our models over the others used for the Caatinga is due to the consideration of WAI, which previously had not been considered in calibrations for the Caatinga, and the temporal variations of LAI, which allowed us to create more generalist models that can be used during different phenological stages of the Caatinga vegetation.

5. Acknowledgements

We thank CAPES (Brazilian Coordination for the Improvement of Higher Level Personnel) for funding this study through the project PVE A103/2013, FACEPE (*Fundação de Amparo a Ciência e Tecnologia do Estado de Pernambuco*) for funding this through the projects FACEPE APQ 0646-9.25/16 and FACEPE APQ 0062-1.07/15 (Caatinga-FLUX), and CNPq (National Council for Scientific and Technological Development of Brazil) for funding this through the project 402834/2016-0 - CNPq Universal 01/2016. This work is also supported by the UK/Brazil Nordeste project, funded jointly through the UK Natural Environment Research Council (NE/N012526/1 ICL and NE/N012488/1 UoR) and FAPESP (São Paulo Research Foundation) (FAPESP 2015/50488-5).

6. References

Ab’Saber, A.N., 1974. O dominio morfoclimático Semi-Árido das caatingas brasileiras. Geomorfologia 1–39.

Alvares, C.A., Stape, J.L., Sentelhas, P.C., de Moraes Gonçalves, J.L., Sparovek, G., 2013. Köppen’s climate classification map for Brazil. Meteorol. Zeitschrift 22, 711–728. doi:10.1127/0941-2948/2013/0507

Arnold, J.G., Srinivasan, R., Muttiah, R.S., Williams, J.R., 1998. Large-area hydrologic modeling and assessment: Part I. Model development. J. Am. Water Resour. Assoc. 34, 73–89. doi:10.1111/j.1752-1688.1998.tb05961.x

Bastiaanssen, W., 1998. Remote sensing in water resources management: the state of the art, IX. ed. International Water Management Institute (IWMI), Colombo, Sri Lanka.

Bieger, K., Arnold, J.G., Rathjens, H., White, M.J., Bosch, D.D., Allen, P.M., Volk, M., Srinivasan, R., 2017. Introduction to SWAT+, a completely restructured version of the Soil and Water Assessment Tool. JAWRA J. Am. Water Resour. Assoc. 53, 115–130. doi:10.1111/1752-1688.12482

Bonan, G.B., 1995. Land-Atmosphere interactions for climate system models: coupling biophysical, biogeochemical, and ecosystem dynamical processes. Remote Sens. Environ. 51, 57–73. doi:10.1016/0034-4257(94)00065-U

Carter, G., Lucas, K., Blossom, G., Lassitter, C., Holiday, D., Mooneyhan, D., Fastring, D., Holcombe, T., Griffith, J., 2009. Remote sensing and mapping of Tamarisk along the Colorado River, USA: a comparative use of summer-acquired Hyperion, Thematic Mapper and QuickBird data. Remote Sens. 1, 318–329. doi:10.3390/rs1030318

Chen, J.M., Black, T.A., 1992. Foliage area and architecture of plant canopies from sunfleck size distributions. Agric. For. Meteorol. 60, 249–266. doi:10.1016/0168-1923(92)90040-B

Chen, J.M., Rich, P.M., Gower, S.T., Norman, J.M., Plummer, S., 1997. Leaf area index of boreal forests: Theory, techniques, and measurements. J. Geophys. Res. Atmos. 102, 29429–29443. doi:10.1029/97JD01107

Cunha, J., Nóbrega, R.L.B., Rufino, I., Erasmi, S., Galvão, C., Valente, F., 2019. Surface albedo as a proxy for land-cover clearing in seasonally dry forests: Evidence from the Brazilian Caatinga. Remote Sens. Environ. doi:10.1016/j.rse.2019.111250

Fotis, A.T., Morin, T.H., Fahey, R.T., Hardiman, B.S., Bohrer, G., Curtis, P.S., 2018. Forest structure in space and time: Biotic and abiotic determinants of canopy complexity and their effects on net primary productivity. Agric. For. Meteorol. 250–251, 181–191. doi:10.1016/j.agrformet.2017.12.251

Frazer, G.W., Lertzman, K.P., Trofymow, J.A., 1997. A method for estimating canopy openness, effective leaf area index, and photosynthetically active photon flux density using hemispherical photography and computerized image analysis techniques. Pacific Forestry Centre, Victoria, B. C.

Galvíncio, J.D., Moura, M.S.B. de, Silva, T.G., Silva, B.B. da, Naue, C.R., 2013. LAI improved to dry forest in Semiarid of the Brazil. Int. J. Remote Sens. Appl. 3, 193. doi:10.14355/ijrsa.2013.0304.04

Gates, D.M., Keegan, H.J., Schleter, J.C., Weidner, V.R., 1965. Spectral properties of plants. Appl. Opt. 4, 11. doi:10.1364/AO.4.000011

Hawkins, D.M., 2004. The problem of overfitting. J. Chem. Inf. Comput. Sci. 44, 1–12. doi:10.1021/ci0342472

Huete, A.., 1988. A soil-adjusted vegetation index (SAVI). Remote Sens. Environ. 25, 295–309. doi:10.1016/0034-4257(88)90106-X

Jacquemoud, S., Baret, F., 1990. PROSPECT: A model of leaf optical properties spectra. Remote Sens. Environ. 34, 75–91. doi:10.1016/0034-4257(90)90100-Z

Jacquemoud, S., Verhoef, W., Baret, F., Bacour, C., Zarco-Tejada, P.J., Asner, G.P., François, C., Ustin, S.L., 2009. PROSPECT+SAIL models: A review of use for vegetation characterization. Remote Sens. Environ. 113, S56–S66. doi:10.1016/j.rse.2008.01.026

Jiang, Z., Huete, A.R., Didan, K., Miura, T., 2008. Development of a two-band enhanced vegetation index without a blue band. Remote Sens. Environ. 112, 3833–3845. doi:10.1016/j.rse.2008.06.006

Kiill, L.H.P., 2017. Caracterização da vegetação da reserva legal da Embrapa Semiárido. Doc. 281, Série Documentos.

Knote, C., Bonafe, G., Di Giuseppe, F., 2009. Leaf Area Index specification for use in Mesoscale Weather Prediction Systems. Mon. Weather Rev. 137, 3535–3550. doi:10.1175/2009MWR2891.1

Knyazikhin, Y., Martonchik, J. V., Diner, D.J. atmosphere-corrected M. data, Myneni, R.B., Verstraete, M., Pinty, B., Gobron, N., 1998. Estimation of vegetation canopy leaf area index and fraction of absorbed photosynthetically active radiation from atmosphere-corrected MISR data. J. Geophys. Res. Atmos. 103, 32239–32256. doi:10.1029/98JD02461

Liu, F., Qin, Q., Zhan, Z., 2012. A novel dynamic stretching solution to eliminate saturation effect in NDVI and its application in drought monitoring. Chinese Geogr. Sci. 22, 683–694. doi:10.1007/s11769-012-0574-5

Machado, C.C.C., 2014. Alterações na superfície do Parque Nacional do Catimbau (PE-Brasil): consolidação dos aspectos biofísicos na definição dos indicadores ambientais do bioma Caatinga. Universidade Federal de Pernambuco.

Magalhães, S.F., Calvo-Rodriguez, S., Do Espírito Santo, M.M., Sánchez Azofeifa, G.A., 2018. Determining the K coefficient to leaf area index estimations in a tropical dry forest. Int. J. Biometeorol. 62, 1187–1197. doi:10.1007/s00484-018-1522-6

Medeiros, E.S. e S., Machado, C.C.C., Galvíncio, J.D., Moura, M.S.B. de, Araujo, H.F.P. de, 2019. Predicting plant species richness with satellite images in the largest dry forest nucleus in South America. J. Arid Environ. 166, 43–50. doi:10.1016/j.jaridenv.2019.03.001

Miranda, R.D.Q., Galvíncio, J.D., Morais, Y.C.B., Moura, M.S.B. de, Jones, C.A., Srinivasan, R., 2018. Dry forest deforestation dynamics in Brazil's Pontal basin. Rev. Caatinga 31, 385–395. doi:10.1590/1983-21252018v31n215rc

Motohka, T., Nasahara, K.N., Miyata, A., Mano, M., Tsuchida, S., 2009. Evaluation of optical satellite remote sensing for rice paddy phenology in monsoon Asia using a continuous in situ dataset. Int. J. Remote Sens. 30, 4343–4357. doi:10.1080/01431160802549369

Mu, Q., Heinsch, F.A., Zhao, M., Running, S.W., 2007. Development of a global evapotranspiration algorithm based on MODIS and global meteorology data. Remote Sens. Environ. 111, 519–536. doi:10.1016/j.rse.2007.04.015

Nackaerts, K., Coppin, P., Muys, B., Hermy, M., 2000. Sampling methodology for LAI measurements with LAI-2000 in small forest stands. Agric. For. Meteorol. 101, 247–250. doi:10.1016/S0168-1923(00)00090-3

Nilson, T., 1971. A theoretical analysis of the frequency of gaps in plant stands. Agric. Meteorol. 8, 25–38. doi:10.1016/0002-1571(71)90092-6

Norman, J.M., 1979. Modelling the complete crop canopy, in: Barfield, B.J., Gerber, J. (Eds.), Modification of the Aerial Environment. American Society of Agricultural Engineers, St. Joseph, USA, pp. 249–277.

Rodriguez, R., Real, P., Espinosa, M., Perry, D.A., 2009. A process-based model to evaluate site quality for Eucalyptus nitens in the Bio-Bio Region of Chile. Forestry 82, 149–162. doi:10.1093/forestry/cpn045

Rouse, J.J.W., Haas, R.R.H., Schell, J.J.A.J., Deering, D.W., Harlan, J.C., 1974. Monitoring the vernal advancement and retrogradation (greenwave effect) of natural vegetation, NASA/GSFC Type III Final Report. NASA Goddard Space Flight Centre, Greenbelt, USA.

Shao, J., 1993. Linear model selection by Cross-Validation. J. Am. Stat. Assoc. 88, 486. doi:10.2307/2290328

Silva, G.C., Sampaio, E.V.D.S.B., 2008. Biomassas de partes aéreas em plantas da caatinga. Rev. Árvore 32, 567–575. doi:10.1590/S0100-67622008000300017

Silva, J.M.C., Leal, I.R., Tabarelli, M., 2017. Caatinga: The largest tropical dry forest region in South America. Springer International Publishing, Cham, Switzerland. doi:10.1007/978-3-319-68339-3

Stenberg, P., 1996. Correcting LAI-2000 estimates for the clumping of needles in shoots of conifers. Agric. For. Meteorol. 79, 1–8. doi:10.1016/0168-1923(95)02274-0

Tavakoli, H., Mohtasebi, S.S., Alimardani, R., Gebbers, R., 2014. Evaluation of different sensing approaches concerning to nondestructive estimation of leaf area index (LAI) for winter wheat. Int. J. Smart Sens. Intell. Syst. 7, 337–359. doi:10.21307/ijssis-2017-659

Teixeira, A.H. de C., Bastiaanssen, W.G.M., Ahmad, M.D., Moura, M.S.B., Bos, M.G., 2008. Analysis of energy fluxes and vegetation-atmosphere parameters in irrigated and natural ecosystems of semi-arid Brazil. J. Hydrol. 362, 110–127. doi:10.1016/j.jhydrol.2008.08.011

Verhoef, W., 1985. Earth observation modeling based on layer scattering matrices. Remote Sens. Environ. 17, 165–178. doi:10.1016/0034-4257(85)90072-0

Verhoef, W., 1984. Light scattering by leaf layers with application to canopy reflectance modeling: The SAIL model. Remote Sens. Environ. 16, 125–141. doi:10.1016/0034-4257(84)90057-9

Weiss, M., Baret, F., Smith, G.J., Jonckheere, I., Coppin, P., 2004. Review of methods for in situ leaf area index (LAI) determination Part II. Estimation of LAI, errors and sampling. Agric. For. Meteorol. 121, 37–53. doi:10.1016/j.agrformet.2003.08.001

Xu, Q.-S., Liang, Y.-Z., 2001. Monte Carlo cross validation. Chemom. Intell. Lab. Syst. 56, 1–11. doi:10.1016/S0169-7439(00)00122-2

Yang, W., Tan, B., Dong Huang, Rautiainen, M., Shabanov, N.V., Wang, Y., Privette, J.L., Huemmrich, K.F., Fensholt, R., Sandholt, I., Weiss, M., Ahl, D.E., Gower, S.T., Nemani, R.R., Knyazikhin, Y., Myneni, R.B., 2006. MODIS leaf area index products: from validation to algorithm improvement. IEEE Trans. Geosci. Remote Sens. 44, 1885–1898. doi:10.1109/TGRS.2006.871215

Zar, J.H., 1996. Biostatistical Analysis, 3rd ed. Prentice Hall, Upper Saddle River.

Zhao, D., Huang, L., Li, J., Qi, J., 2007. A comparative analysis of broadband and narrowband derived vegetation indices in predicting LAI and CCD of a cotton canopy. ISPRS J. Photogramm. Remote Sens. 62, 25–33. doi:10.1016/j.isprsjprs.2007.01.003